Waterjet System Performance and Cavitation Test Procedures

Jie Dang[1], Runwen Liu[2] and Christiaan Pouw[1]

[1]The Maritime Research Institute Netherlands (MARIN), Wageningen, The Netherlands
[2]China Ship Scientific Research Center (CSSRC), Wuxi, China

ABSTRACT

Different from marine propeller designs, which undergo standard stock and design propeller test programmes with detailed assessments of the final design (for the overall propulsive efficiency, the cavitation performance and the pressure fluctuations, etc.), waterjet systems of a final design are seldom tested for their system characteristics, the intake loss and the cavitation performance. It could be both due to economical reasons that waterjet system tests are relatively expensive. It could also be due to technical reasons, such as, that the operating point of a waterjet system does not vary too much for different operational conditions. This means that it performs also very well for all other operational (off-design) conditions once a waterjet system is well-designed for its design condition. However in practice, mismatching of power absorption and shaft rotational rate, and cavitation erosion, are now and then found after the sea trials of the waterjet propelled ships. Remedial action is needed then. In some cases, removing cavitation erosion can be rather difficult and simple modifications may not solve the problem.

In order to prevent those kinds of problems from the early design stage, waterjet system performance and cavitation tests of the final design are strongly recommended. Taking example of a Fast River Passenger Ferry, test procedures are discussed in detail in the present paper. The scale effects and the extrapolation method are also addressed. The results provide a good data set for CFD validation too.

Keywords

Waterjet, Pump, Performance, Cavitation, Procedures

1 INTRODUCTION

The Waterjet Group of the 21st International Towing Tank Conference (ITTC) concluded already in 1996 that model self-propulsion tests were required to make reliable predictions of the performance of waterjet propelled crafts (Kruppa 1996): 'Performance predictions, based on resistance test only, may lead to serious error.' However, waterjet propelled ships are still being built without conducting tests for self-propulsion, waterjet system and pump performance for the final intake, impeller and stator designs. Serious problems are often encountered after sea trials for unsatisfactory ship performance, for mismatching of the power absorption of the pump, and even more seriously – for cavitation erosion on the impeller blades.

After great effort in the last decades of the Special Committees of the ITTC on Waterjet Test Procedures (van Terwisga 2005), the ITTC Recommended Procedures and Guidelines have been established and continuously improved (ITTC 2005, 2011). It is the intention of the ITTC that the procedures and guidelines are 'kept as generic as possible'. No detailed test procedures and extrapolation methods, such as that for ships with marine propellers – the ITTC 1978 method, have been specified. The implementation of the ITTC procedures for waterjet tests has been left for individual test facilities.

In the last decades, self-propulsion tests of waterjet propelled ships were carried out very frequently in the Deep Water Towing Tank of MARIN, ranging from ships with low speed displacement monohulls to high speed catamaran, trimaran and planing crafts. Ships with hybrid propulsion systems were also often tested, where the waterjets were mainly used as boosters. Occasionally, waterjet systems were tested for their system and cavitation performance on top of the Large Cavitation Tunnel at MARIN by using a bypass (Kooiker et al. 2003). Much experience has been gained with the test set-ups, the use of the equipment, the test procedures, the analysis of the results, the scale effects and the extrapolation method.

Taking the 15m Fast River Passenger Ferry as an example, designed by CSSRC and tested at MARIN, the implementation of the ITTC test procedures will be discussed in this paper. The complete test programs consisted of the resistance test, the self-propulsion test by using stock waterjets, and the large scale waterjet system performance tests including cavitation inception tests and cavitation observations. The focus of the present paper is on the waterjet system test procedures in the cavitation tunnel and the extrapolation of the results.

Regarding the fact that the community on waterjets is rather small and the number of experts on waterjet system performance tests are very limited (Arén et al. 1993, Hoshino and Baba 1993, Fujisawa 1995, Brandner and Walker 2001, Kooiker et al. 2003, Donnelly and Gowing 2008, Chesnakas et al. 2008 & 2010, Tan et al. 2012 & 2012), the understanding on the physics and the scale effects of a waterjet system is still very limited. Compared to that of the marine propellers, experience with waterjet system tests are built up slowly.

The goal of the present paper is two-fold: To share the experience on waterjet system model tests and the test procedures, and to build a reliable data set for validation of CFD simulations.

2 SHIP AND WATERJET SYSTEMS

The subject ship is a 15m long Fast River Passenger Ferry fitted with two 230kW waterjet systems with flush intakes, sailing at a top speed over 25 knots. A scaled ship model has been manufactured with light wooden frames and Plywood planking, in order to reduce the weight of the model. The scale ratio is 1 to 3.571, resulting in a ship model of 4.2 meters. The model is equipped with two Hamilton stock waterjet pumps fitted to exactly-scaled waterjet intake geometry and nozzle, see Figure 1.

Figure 1 Self-propulsion tests with stock waterjets.

Resistance and propulsion tests were carried out according to the ITTC standard procedure (ITTC 2011), including boundary layer measurements before the intake (with a closed intake) and the bollard pull calibration for the flow rate before carrying out the propulsion test. The effective jet system power P_{JSE} and propulsion factors were obtained, as selected in Table 1 at 15 knots, 20 knots and the full power free sailing speed of 25.69 knots.

Table 1 Self-propulsion test results

Vs Knots	Q/unit m^3/s	IVR -	P_{JSE}/unit kW	PD/unit kW	Cp -
25.69	0.5381	0.7177	205.1	230	43.76
20.00	0.4631	0.7942	134.0	152	45.26
15.00	0.4003	0.9158	89.5	102	47.04

To arrive at the shaft delivered power at the impeller P_D, the pump efficiency in uniform free stream condition η_{P_0}, the installation efficiency η_{inst} and the duct efficiency η_{duct} must be known so that,

$$\eta_D = \frac{P_E}{P_D} = (1-t)\frac{\eta_{\mathrm{eI}}}{\eta_{\mathrm{mI}}}\eta_{\mathrm{I}}\eta_{\mathrm{duct}}\eta_{\mathrm{P_0}}\eta_{inst}\,. \qquad (1)$$

At the stock waterjet propulsion test stage, the waterjet system efficiency $\eta_{js} = \eta_{duct}\,\eta_{P_0}\,\eta_{inst}$ is often provided by the waterjet vendors. The shaft power and the power loading coefficient C_P at a given sailing condition can then be determined, which are listed in Table 1, where,

$$C_P = P_D \Big/ \left(\frac{1}{2}\rho \left(\frac{Q}{D_P^{\,2}} \right)^3 \frac{1}{4}\pi D_P^{\,2} \right). \qquad (2)$$

Due to the flow distortion to the pump, caused by the waterjet ducting system and the shaft, the installed pump efficiency η_P is somewhat lower than the uniform free stream efficiency η_{P_0}. For a 90° bended circular duct, 4% losses have been found, resulting in an installation efficiency η_{inst} of 0.96 (Kruppa 1993). These losses are typically only 2% for a flush mounted waterjet pump as found by Kooijker et al. (2003).

Practically, pump test for the uniform free stream efficiency η_{P_0} may not be necessary if the pump efficiency in the installed condition η_P can be measured correctly.

In order to determine the waterjet system efficiency η_{js}, waterjet system test should be carried out, which will be discussed in detail in the rest of the paper.

3 TEST SET-UP

After the propulsion test with the stock waterjets, a final waterjet system with a flush intake and a mixed-flow pump were designed for this ferry. The ducting system was designed by a parametric geometry modelling with mathematical expressions for the intake curved surfaces which were coupled to a commercial CAD program to generate the 3-D geometry (Liu 2010) - a method similar to Purnell (2008). The mixed-flow pump was selected from a standard series and scaled for the present ship.

3.1 Waterjet system model

A large waterjet system model was built according to the final design to a scale of 1:1.5, see Figure 2, which consisted of an aluminium block with an intake ducting system, a transparent pump house, a bronze stator and a bronze impeller, which was connected by the shaft to the shaft torque sensor. This model is mounted flush in the top ceiling of the test section of the Large Cavitation Tunnel of MARIN (Figure 3, Figure 4). The nozzle of the waterjet was connected to a bypass and the water was led back to the cavitation tunnel in a downstream section. In the bypass, the flow rate was controlled by a valve and measured by a flow rate meter. A detailed description of the tunnel and the bypass can be found in Kooiker et al. (2003).The main dimensions of the waterjet system model are listed in Table 2 and the main dimensions of the impeller and the stator are provided in Table 3.

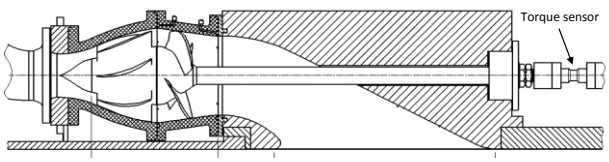

Figure 2 Test set-up of waterjet model, torque sensor.

Table 2 Main dimensions - waterjet system

Main dimensions		Full scale	Model scale	
Pump diameter (max)	D_p	328.304	218.869	mm
Effective nozzle diameter	D_N	152.867	101.871	mm
Nozzle area	A_N	0.01835	0.00816	m^2
Pump inlet area	A_4	0.05657	0.02514	m^2
Pump max. area	A_5	0.05224	0.02322	m^2
Height z0	z0	0.6750	0.4500	m
Height z1	z1	0.7530	0.5020	m
Height z2	z2	0.8226	0.5484	m
Height z3	z3	1.0418	0.6945	m
Shaft height z4, z5	z4, z5	0.9300	0.6200	m

Table 3 Main dimensions - impeller and stator

Impeller/stator models	Symbol	Impeller	Stator	Unit
Diameter (max.)	D	211.09	216.60	mm
Diameter (Min.)	D	195.54	115.73	mm
Boss-diameter ratio	d/D_P	0.6188	0.6188	-
Number of blades	Z	3	7	-
Impeller/Stator models material	-	bronze	bronze	-

Slightly different from the ITTC procedures, the pump head was measured between the inlet of the pump and the maximum diameter of the pump house, by 4 holes at each location which were connected to a common channel and measured as two average pressures by pressure sensors through tube connections. This was due to the difficulties to drill holes at the end of the stator and to measure the pressure there, as proposed by the ITTC. The details of the pressure holes, their locations and the channels are drawn and shown in the photo in Figure 5.

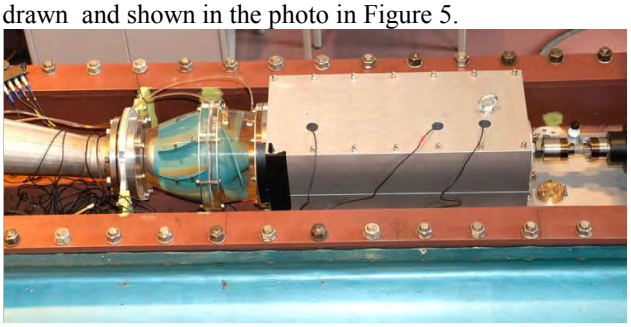

Figure 3 Waterjet system mounted on the top ceiling of the Large Cavitation Tunnel at MARIN.

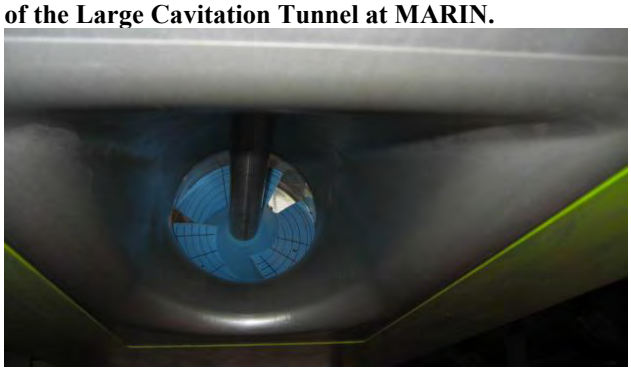

Figure 4 Intake of the waterjet system model.

To simulate the boundary layer to the waterjet intake, serrated strips can be installed upstream of the intake on the ceiling of the cavitation tunnel, Kooiker et al. (2003). For the present project however, the boundary layer was not simulated by an artificial technique for the sake of CFD validation in the future.

In order to trip the turbulent boundary layer flow on the impeller blades, to generate enough nuclei for cavitaion inception and for stable sheet cavitaiton on the blades, carborundum grains of 60μm were applied to all of the leading edges of the impeller blades on both pressure side and suction side on 3 mm wide strips.

On the ramp of the intake, three additional pressure sensors (Figure 3, Figure 6) have been mounted flush to the ramp surface to follow the changes in the pressure along the ramp and to indicate possible scale effects when testing at different tunnel speeds, shaft rotational rates and *IVR* ratio's.

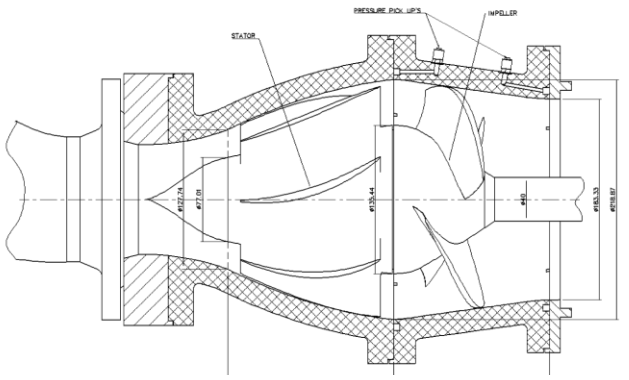

Figure 5 Details of pump and pressure pick-up's.

For the sake of convenience on numbering the pressure pick-up's, the stations of the tested waterjet system is defined differently from the ITTC standard definition, as shown in Figure 6.

During the tests, the static mean pressures are measured at point p1 to p5. In the meantime, the tunnel pressure p0 is also measure at the central line of the tunnel. To arrive at the static pressure at p0', p4' and p5', the pressure ρgz from the water column has been added to p0, p4 and p5, respectively.

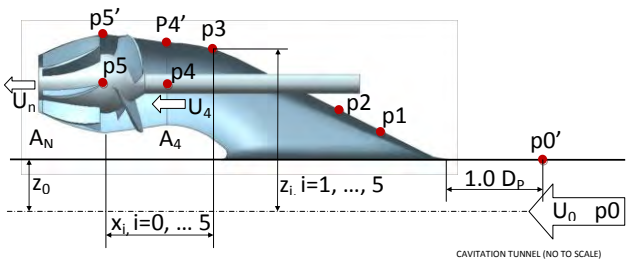

Figure 6 Pressure pick-ups and station numbers.

In order to accurately calculate the pump head and the intake ducting system loss, a detailed flow survey should be carried out by using PIV or LDV systems, both at the capture area of the intake (around station 0') and the inlet of the pump (at station 4).

At the intake, without boundary layer simulated for the present test, the ingested flow can be treated as uniform flow because the intake is very close to the end of the contractor of the cavitation tunnel where the boundary layer is very thin. However, the non-uniformity of the flow at the inlet of the pump can result in much higher

integrated energy flux than that calculated by the mean velocity based on the flow rate and the cross section area (Scherer et al. 2001, Chesnakas et al. 2008). The bias error due to the non-uniformity of the flow at the inlet of the pump may give small errors to the calculation of the pump head because the static pressure head for a mixed-flow pump is dominant. However, these errors can result in large discrepancies on calculating the intake loss. Also important is to determine correctly the capture area, where CFD plays important roles.

LDV measurements have been carried out at MARIN in the past, however not for this present waterjet system tests.

To observe cavitation on the impeller blades and on the inside of the pump house, both normal video recordings in stroboscope light as well as high speed video recordings (up to 1850 frames per second) in continuous illumination have been carried out by looking through the transparent pump house. To observe the possible cavitation at the lip region of the intake, a camera looking through the bottom window of the tunnel or an underwater camera can be used, as shown in Figure 4. However, the intake lip cavitation was not the focus of the present model tests.

4 TEST PROCEDURES AND RESULTS

In order to extrapolate the results of the waterjet system performance test correctly to full scale, waterjet system performance tests should be carried out at various combinations of tunnel water speeds, shaft rotational rates and *IVR* ratio's to understand the Reynolds effects.

For the present ferry, three *IVR*'s (0.7177, 0.7942 and 0.9158) were chosen for the studies, corresponding to the vessel speed of 25.69 knots, 20 knots and 15 knots (Table 1), respectively. Five tunnel water speeds were used during the tests. The tests were carried out in such a way that the tunnel water speed was first set to a constant value; for each shaft rotational rate, the valve on the bypass was used to adjust the flow rate until the required *IVR* was reached according to the flow rate meter.

The complete test matrix is shown in Table 4, where the tunnel speed has been set from 3 m/s to 7 m/s while the shaft rotational rate has been run in steps on a range from minimum 790 RPM to maximum 2300 RPM. Due to the head loss in the bypass, the tests could not be conducted at high *IVR*'s with high flow rate for tunnel speeds of 6 and 7 m/s. An additional support pump in the bypass is obviously needed in order to overcome the bypass head loss. To prevent the influence of cavitation on the waterjet system performance, a high pressure (> 2 bars) in the tunnel was applied to suppress cavitation.

Table 4 Waterjet system performance test conditions

Tunnel water velocity U_0	Impeller shaft rotational rate n (min. - max.)	IVR's for every U_0 and n
3	790 RPM – 1630 RPM	0.7177, 0.7942, 0.9158
4	1035 RPM – 1960 RPM	0.7177, 0.7942, 0.9158
5	1300 RPM – 2085 RPM	0.7177, 0.7942, 0.9158
6	1540 RPM – 2330 RPM	0.7177, 0.7942
7	1800 RPM – 2300 RPM	0.7177

4.1 Pump performance

Two examples of the pump performance test results at tunnel speeds of 3 and 5 m/s for three *IVR*'s are plotted in Figure 7 and 8, respectively.

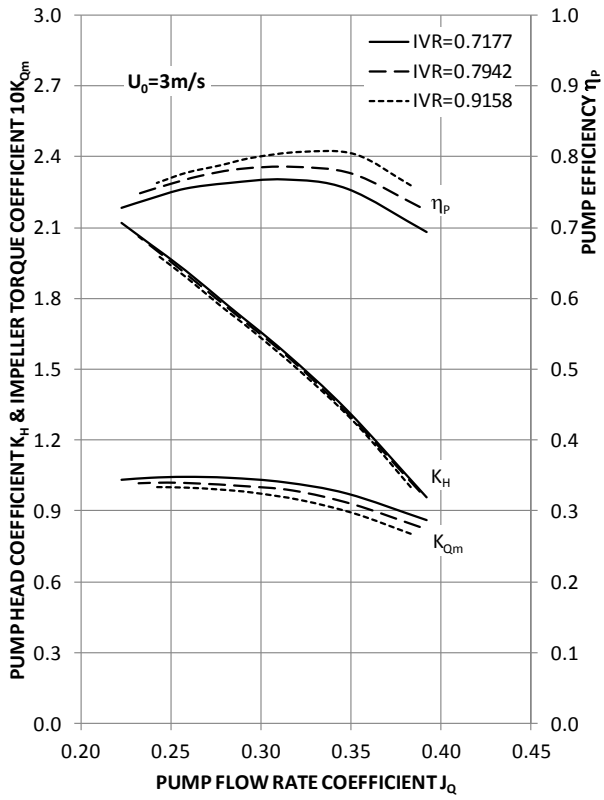

Figure 7 Pump performance characteristics (3m/s).

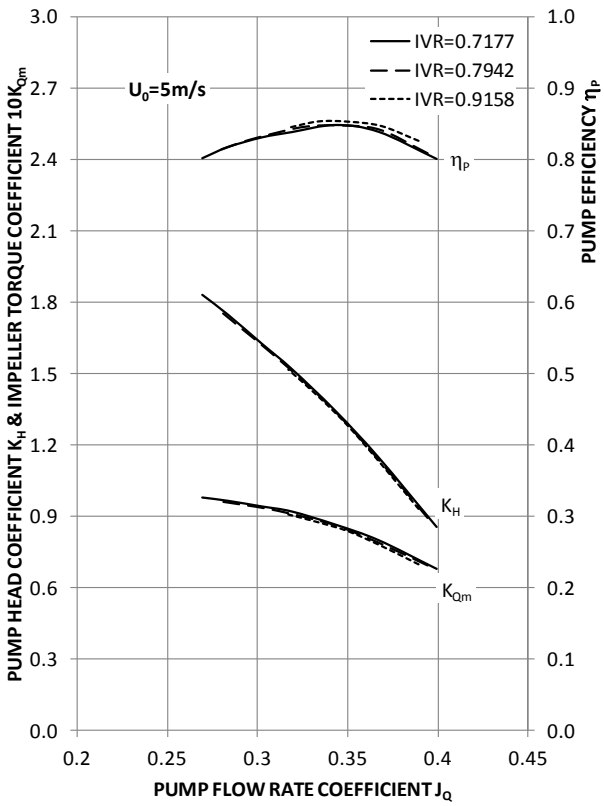

Figure 8 Pump performance characteristics (5m/s).

In the figures, the flow rate coefficient J_Q, the pump head coefficient K_H, the impeller torque coefficient K_{Qm} and the pump efficiency η_P were defined as,

$$J_Q = \frac{Q}{nD_P^{\,3}};\ K_H = \frac{gH}{n^2 D_P^{\,2}};\ K_{Qm} = \frac{Q_m}{\rho n^2 D_P^{\,5}};\ \eta_P = \frac{J_Q K_H}{2\pi K_{Qm}}. \quad (3)$$

Here the pump head is the total head, as defined by ITTC (2005), including the static part measured as the mean pressure at p4 and p5 and the dynamic part calculated by using the mean velocities based on the flow rate and the cross section areas.

It is seen from Figure 7 that at a low tunnel speed of 3 m/s the pump characteristics depend clearly on *IVR*'s, where *IVR* is defined as the ratio of the mean velocity at the inlet of the pump U_4 to the tunnel velocity U_0. This *IVR* dependency comes mainly from the impeller shaft torque. At 5 m/s as shown in Figure 8, the pump characteristics become independent of the *IVR*'s, however.

In order to investigate the Reynolds effects on the pump characteristics, the measured data were interpolated at given flow rate coefficients J_Q's and plotted against the duct Reynolds numbers and the impeller blade chord Reynolds numbers for the pump head and the shaft torque in Figure 9 and Figure 10, respectively, where the Reynolds numbers were defined as,

$$\mathrm{Re}_D = \frac{QD_4}{\nu A_4};\quad \mathrm{Re}_C = \frac{V_{tip} C_{tip}}{\nu}. \quad (4)$$

Figure 9 shows the pump head coefficients that are neither Reynolds numbers nor *IVR*'s dependent in the range from 3 m/s to 7 m/s of tunnel water speeds. When checked the test conditions with the material and the surface roughness levels of the duct model with the Moody Diagram, it is seen that the duct flow at the pump inlet is already fully-turbulent at 3 m/s. This may explain why the pump head is independent of the Reynolds numbers.

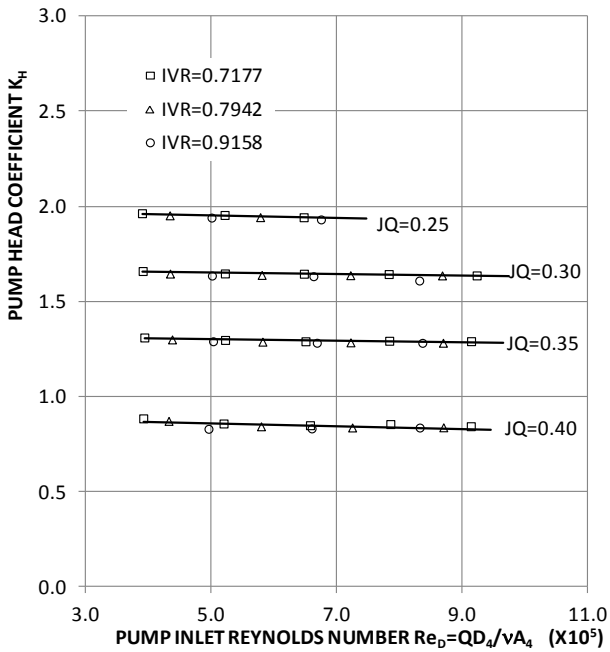

Figure 9 Reynolds effects on pump head coefficients.

Although the shaft torque coefficients are also independent of the *IVR*'s, as shown in Figure 10, they are highly dependent on the impeller chord Reynolds numbers. This is rather similar to that of the marine propellers. In addition, the tests covered already a rather high chord Reynolds numbers in the range from 2×10^6 to 5×10^6. The results in Figure 10 show also that the shaft torque becomes less Reynolds dependent from a rather high Reynolds number around 4×10^6. This means that a reliable waterjet system performance tests should be carried out at high shaft rotational rates.

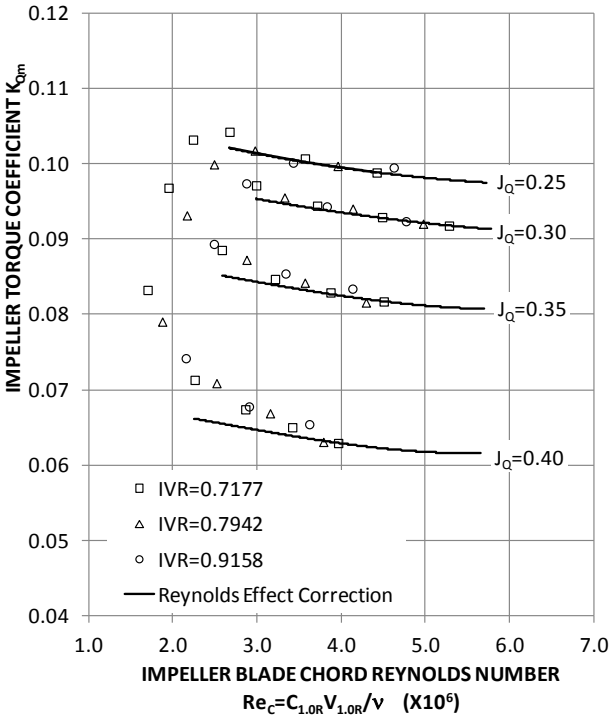

Figure 10 Reynolds effects on impeller torque coefficients.

To extrapolate the model scale results to full scale, Lerbs' method (1951), as adopted by the ITTC for extrapolating the propeller open water characteristics, can be used, where the corrections are only applied to the impeller torque coefficients as,

$$\Delta K_{Qm} = C_1 \times \Delta C_D \times \frac{ZC_{tip}}{D_P}, \quad (5)$$

where C_1 is a constant which can be determined by fitting the results to the measurements as shown in Figure 10 by the solid curves. For the present mixed flow pump, a value of 1.70 has been found for the best fitting.

The drag correction is defined here as,

$$\Delta C_D = 2\left[1 + 2\frac{t_{\max}}{C}\right]\left(C_{f\_\mathrm{ship}} - C_{f\_\mathrm{model}}\right), \quad (6)$$

and the Prandtle and von Kármán original friction coefficient for turbulent flow can be used. In addition, surface roughness can be taken into account,

$$C_{f\_\mathrm{model}} = 0.074\,\mathrm{Re}_{C\_\mathrm{model}}^{\ -1/5}, \quad (7)$$

$$C_{f\_\mathrm{ship}} = \max\left\{\begin{array}{l} 0.074\,\mathrm{Re}_{C\_\mathrm{ship}}^{\ -1/5} \\ \left(1.89 + 1.62\log\dfrac{C_{\mathrm{tip\_ship}}}{k_s}\right)^{-2.5} \end{array}\right. . \quad (8)$$

4.2 Pressure distribution

The pressure distribution along the ramp of the waterjet intake provides insights of the possible Reynolds effects on the intake duct loss, the pressure levels on the cavitation and the indication of possible flow separation. The following definition has been used for the pressure coefficients,

$$C_p = \frac{p_i - \rho g(z_i - z_{0'}) - p_{0'}}{1/2\rho U_0^2}, \qquad (9)$$

where all pressure sensors at p_i were set to zero at the beginning of each test when the tunnel water speed was zero and the pressure at the centreline of the tunnel was at atmospheric pressure.

One of the typical examples of the pressure distribution on the ramp is plotted in Figure 11 at the tunnel water speed of 4 m/s, where the dots are the measured values and the curves are trend lines to show the possible variation of the pressure along the ramp surface. The results show a strong *IVR* dependency for the pressure distributions, especially at the place close to the inlet of the pump. This phenomenon is the same at all other tested conditions with the tunnel water speeds ranging from 3 m/s to 7 m/s.

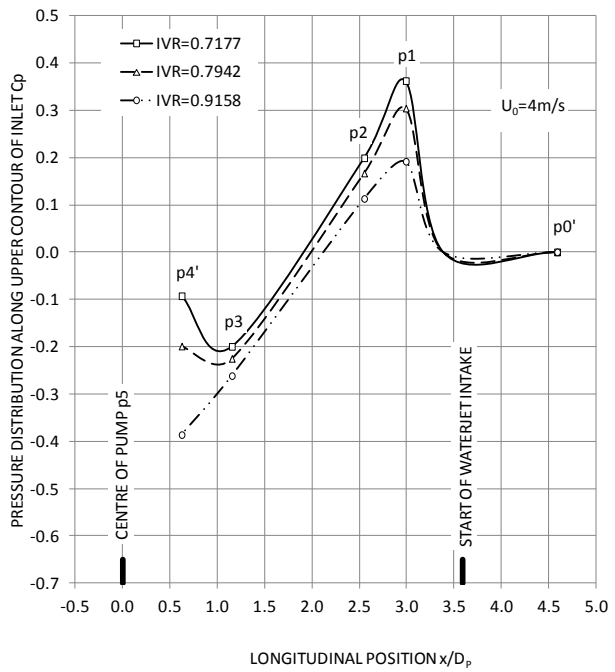

Figure 11 *IVR* influence on ramp pressure distribution

To illustrate the Reynolds effect on the pressure distribution on the ramp of the intake, the pressure distributions are plotted in Figure 12 for one *IVR* but tested at different tunnel water speeds from 3 m/s up to 7 m/s. This covers the duct Reynolds numbers from 3.9×10^5 to 9.2×10^5. It is shown that the pressure distribution is approaching asymptotically to a converged level when the tunnel water speed is increased to 7 m/s and the duct Reynolds number is increased to a level close to 10^6 accordingly. The pressure distribution at 3 m/s is completely different from that at 7 m/s. There are two implications:

First, the duct loss is strongly Reynolds dependent. To get a good estimation of the duct loss, tests at high duct Reynolds numbers are essential. This observation is different from those found by previous studies (Fujisawa 1995), which will be discussed further in the next section,

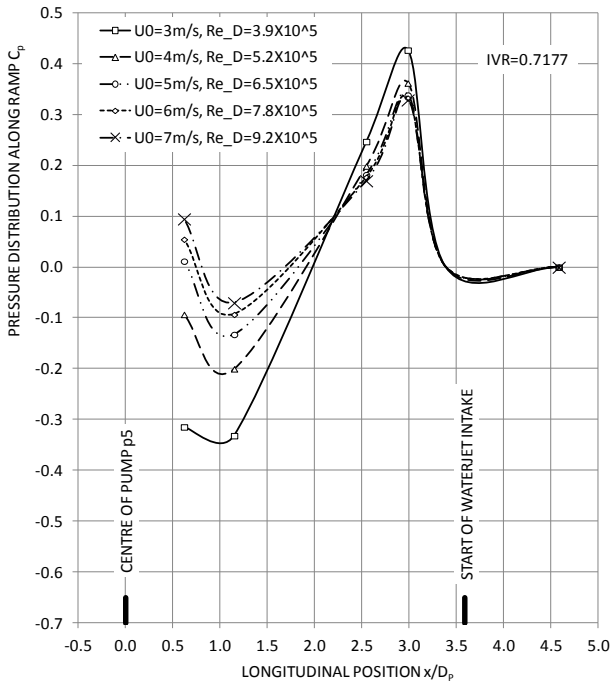

Figure 12 Reynolds effects on pressure on the ramp.

Secondly, the change of the pressure levels at the inlet of the pump at different tunnel water velocities will result in different cavitation numbers during the cavitation inception and observations tests. Good cavitation tests can only be guaranteed when the tests are carried out at high duct Reynolds numbers.

4.2 Intake loss

The waterjet system performance tests are often used to determine the intake loss too. However, detailed flow surveys must be carried out before an accurate calculation of the loss can be carried out, as discussed before and intensively by Scherer et al. 2001 and Chesnakas et al. 2008. In addition, the boundary layer has to be simulated and the intake capture area must be known. This imposes some difficulties on the tests of intake loss.

Flow surveys by using LDV measurement have been carried out previously at MARIN for other projects, however it is not carried out for the present project due to limitation of the funding.

The intake duct loss coefficient is defined as,

$$\varsigma_{04} = \frac{E_0 - E_4}{1/2\rho U_0^2 Q}. \qquad (10)$$

Non-uniform flow contains always higher kinetic energy flux than that of uniform flow at the same momentum flux. Small non-uniformity, say 10% velocity variation, may result in only 1% kinetic energy increase. However, 100% variations (suppose half of the duct is blocked), will result in 2 times more kinetic energy than uniform flow.

The distortion of the flow by the intake has been found to be large at the pump inlet, which depends on the intake design. It can result in an energy flux deviation from uniform flow by more than 20% (Scherer et al. 2001).

To study the Reynolds effects on the intake loss however, an apparent intake loss coefficient can be used,

$$\bar{\varsigma}_{04} = \frac{P_0 - P_4}{1/2\rho U_0^2} \tag{10}$$

where P is the total pressure at station 0 and 4, assuming uniform flow at both stations.

The apparent duct loss coefficients are plotted against the flow rate coefficients in Figure 13 for all tested conditions. The figure shows that the apparent intake losses are not strongly affected by the loadings of the impeller. The levels remain the same for different flow rate coefficients J_Q's. However, they depend strongly on the tunnel water speeds and the *IVR*'s.

The duct loss levels are calculated unrealistically high at 20% to 30%. This is regarded as the influence of the non-uniformity of the flow at station 4, rather than the scale effects of the model test itself.

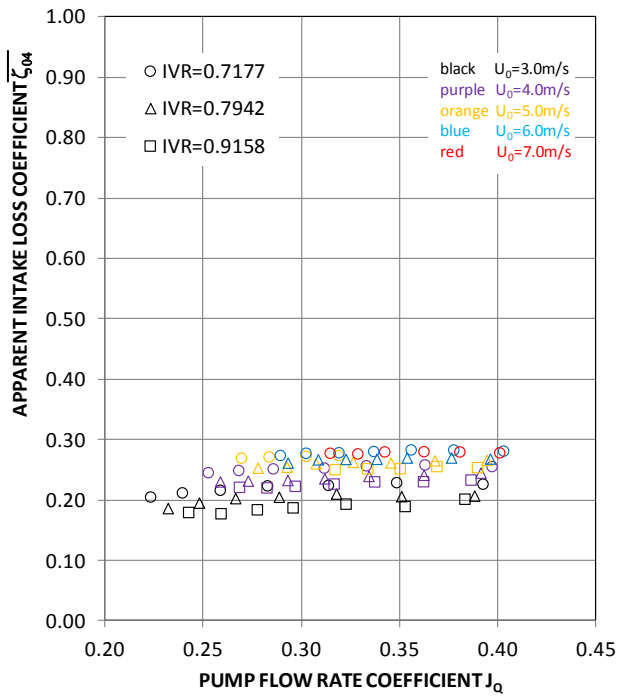

Figure 13 Intake losses at different speeds and *IVR*'s.

When the measured apparent duct loss coefficients are plotted against the duct Reynolds numbers, a clear asymptotic convergence can be seen, as shown on Figure 14. It seems that a duct Reynolds number up to 10^6 is needed to get a converged results. The correction of the test results to full scale remains still a challenge.

It is also seen in the figure that the scatters of the measured apparent duct losses at different loadings of the impeller (different flow rate coefficients J_Q's) are also reducing with the increase of the duct Reynolds numbers.

It should also be pointed out that flow surveys at different cross sections are needed in order to determine the capture area at the intake. Instead, CFD simulations may provide better solutions on the duct losses.

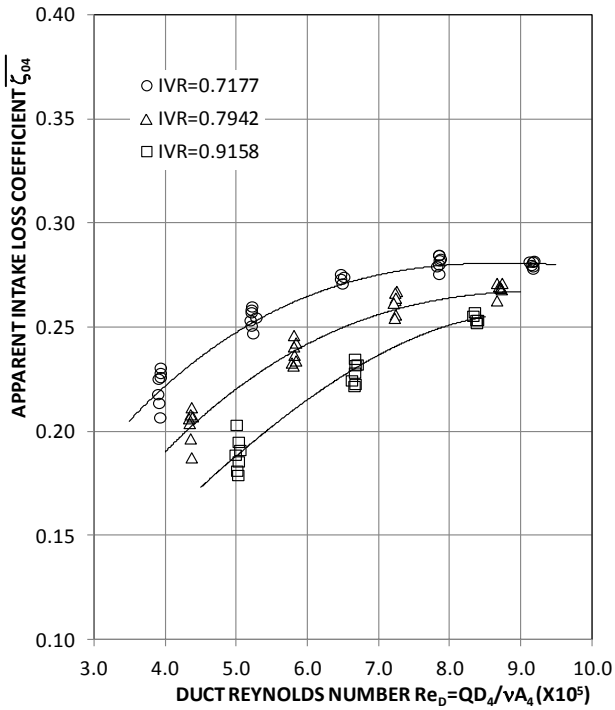

Figure 14 Reynolds effects on intake duct losses.

4.3 Determine operating point

The test method proposed by the ITTC is a momentum based method. The direct results of the tests are the flow rate Q and the required effective jet system power P_{JSE} at given ship speed. It is hence easy to use a power loading coefficient to find the operating point, rather than the thrust loading coefficient as for propellers.

The pump characteristics are extrapolated to full scale. Corrections are only applied to the torque coefficients according to Equation 5. The pump head scale effects are neglected. The full-scale shaft torques are calculated by,

$$K_{Qs} = K_{Qm} + \Delta K_{Qm}\,. \tag{11}$$

An additional 1.6% correction were applied to account for the direct losses due to the roughness applied at the leading edges based on experience and a 0.5% correction was applied to account for the friction losses of the bearings. The full scale pump characteristics are plotted in Figure 15. Also plotted in the figure is the power loading coefficient curve calculated by,

$$C_P = 16K_{Qs} / J_Q^3\,. \tag{12}$$

By matching the power loading coefficient from the self-propulsion test results (Equation 2) to that of the pump characteristics (Equation 12), the operating point can be determined, as shown in Figure 15 for the full power free sailing condition at 2 × 230kW (25.69 knots). The flow rate coefficient J_Q, the shaft rotational rate n and the pump efficiency in installed condition η_P can be determined.

For the present ship, the pump efficiency is found to be 0.930 at 25.69 knots with a shaft rotational rate of 2920 RPM in full scale.

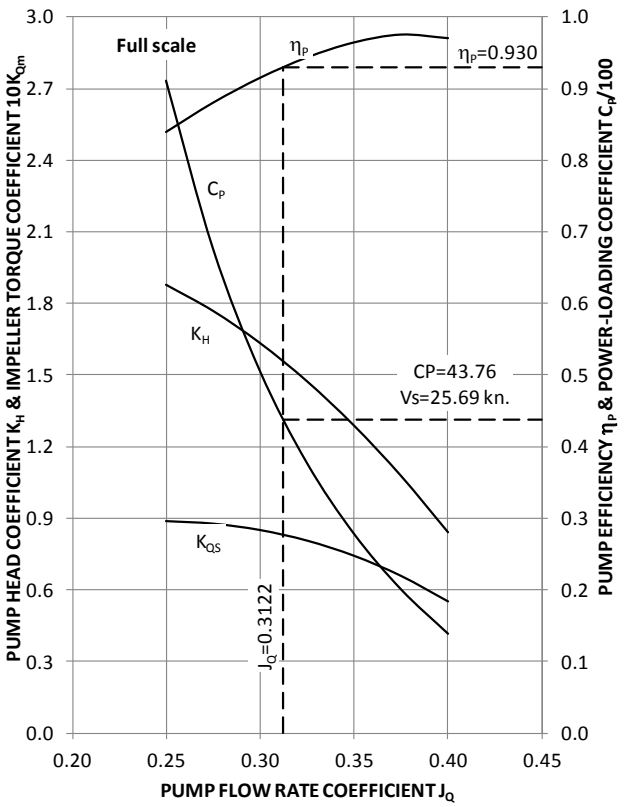

Figure 15 Determine waterjet operating point.

4.4 Cavitation inception tests and extrapolation

During cavitation inception tests of a waterjet system, the tunnel water velocity is often chosen and fixed at a certain speed. The tests are carried out at a given *IVR* value, meaning a fixed flow rate Q when the tunnel water velocity is fixed. The impeller rotational rate is set at a certain RPM and the valve in the bypass is varied until the required flow rate Q is attained. At this condition, the tunnel pressure can be adjusted until cavitation inception takes place. By changing the setting of the shaft rotational rate, inception curves can be determined for various types of cavitation.

The points of inception are determined visually, using stroboscopic illumination that flashes once every revolution. Points of inception are found by establishing the condition in which at least half of the number of blades shows inception in their most sensitive blade positions. Through the measurements, K_{Qm} values are derived in a direct manner at specific suction speed n_{ss}.

In the inception diagram the model inception points are shown in combination with the predicted full-scale K_{Qs}-$1/n_{ss}$ relationship (operation curve). If there would be no scale effects on cavitation inception, the model inception curves are valid for full scale as well. When effective leading edge roughness is applied in the model tests, scale effects are supposed to be absent as far as sheet and bubble types of cavitation are concerned. It is generally accepted that important viscous scale effects are present on the inception of free vortex cavitation.

According to McCormick rule, there is a direct relation between the cavitation inception number and the Reynolds number. For equal angles of attack (equal loading) the cavitation inception number σ_{ni} scales with:

$$\frac{\sigma_{ni\_ship}}{\sigma_{ni\_model}} = \left(\frac{R_{n\_ship}}{R_{n\_model}}\right)^{0.35} \tag{13}$$

where R_n is the Reynolds number of the propeller blade, which is proportional to nD_P^2/ν. It is proposed to be applied to the impeller of a pump as well. This relation becomes then,

$$\left(\frac{1/n_{ss\_ship}}{1/n_{ss\_model}}\right)^{4/3} = \left(\frac{R_{n\_ship}}{R_{n\_model}}\right)^{0.35}. \tag{14}$$

Hence,

$$\frac{1/n_{ss\_ship}}{1/n_{ss\_model}} = \left(\frac{R_{n\_ship}}{R_{n\_model}}\right)^{0.2628}. \tag{15}$$

The final results of the cavitation inception tests are plotted in Figure 16 with $1/n_{ss} \sim K_{Qs}$ relations for various types of cavitations. The area above those curves is a cavitation free zone. Also plotted in this diagram is the operation curve of the waterjet pump.

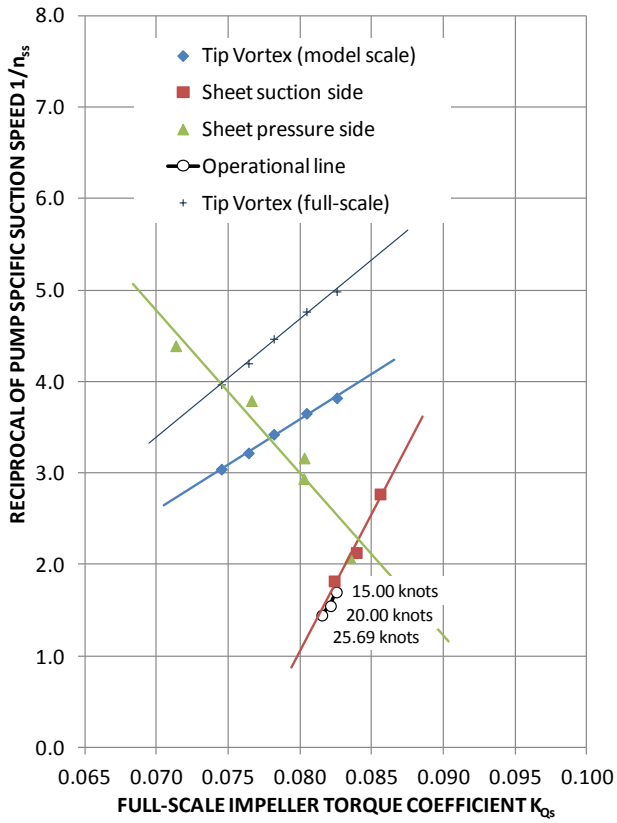

Figure 16 Cavitation inception buckets, extrapolation.

It is seen from Figure 16 that the impeller operates on the edge of suction side cavitation inception while pressure side leading edge sheet cavitation is on the surface of all impeller blades for all operational conditions from 15 knots to the top speed of 25.69 knots. This can be seen in the next section. Also seen from this figure is that the impeller operating points do not vary that much from 15 knots to 25.69 knots. This justifies the common practice of the waterjet vendor's assumption that once a waterjet is well designed for its design operational condition, it will

also work well for off-design conditions. However, this implies also that if it is wrongly designed for the design condition, it is wrong for all operational conditions!

It has also been seen during the cavitation inception tests that the tip gap cavitation inception occurs at almost the same time as the inception of the tip vortex cavitation.

4.5 Cavitation observation - high speed video

Through the transparent pump house, cavitation on the impeller blades and in the complete pump house can be observed by using video camera's with stroboscopic lights and a high speed video camera in continuous illumination. Tests are often carried out at a given operational condition and a given pump specific suction speed. The pump specific suction speed is defined as:

$$n_{ss} = \frac{n\sqrt{Q}}{(gH_{ss})^{3/4}}, \tag{15}$$

where H_{ss} is the pump specific suction head at an arbitrary immersion h_s in full scale defined as,

$$H_{ss} = \frac{p_0 + \frac{1}{2}\rho U_0^2 + \rho g h_s - p_v}{\rho g} \tag{16}$$

in which p_0 is the atmospheric pressure on full scale on the free surface and p_v is the vapour pressure of water.

Since the gravitation is not simulated in the cavitation tunnel without a free surface, the vertical pressure gradient in model scale is not similar to that in full scale. For a cavitation tunnel a rate of rotation for model scale is chosen within practical limits related to the tunnel capacity, the particular test set-up and the ranges of static pressure.

Requiring equal pump specific suction speeds on model and full scale then leads to the pressure to be adjusted in the tunnel. Obviously, at only one horizontal level, the condition of equal pump specific suction speed can be fulfilled. For a waterjet pump, a practical choice for the equal pump specific suction speeds is the impeller tip in the upper most position.

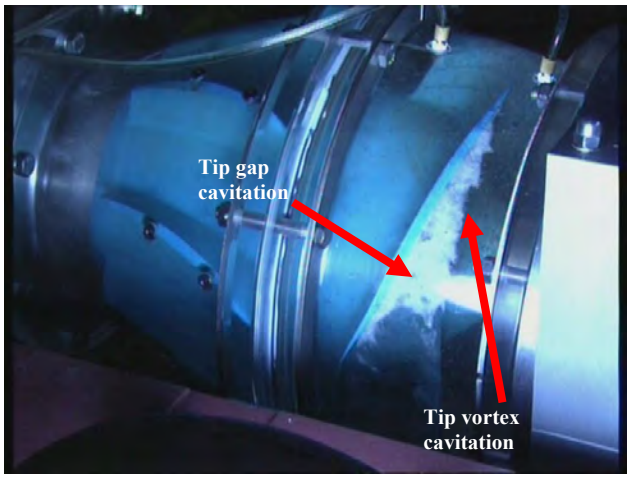

Figure 17 Suction side tip gap and vortex cavitation at full power free sailing speed of 25.69 knots.

For the present ship at full power free sailing condition of 25.69 knots, one typical picture from the cavitation video recordings with stroboscopic light is shown in Figure 17 for the tip gap and vortex cavitation, when the impeller leading edge was passing through the 12 o'clock position. A developed tip vortex cavitation is clearly seen from the leading edge of the tip. Tip gap cavitation was observed in the whole revolution covering the triangular area between the blade tip section and the tip vortex, which initiated at the sharp edge of the tip on the pressure side and developed and connected to the tip vortex cavitation.

No sheet cavitation on the suction side of the impeller was observed, which was in line with the cavitation inception tests discussed in the previous section.

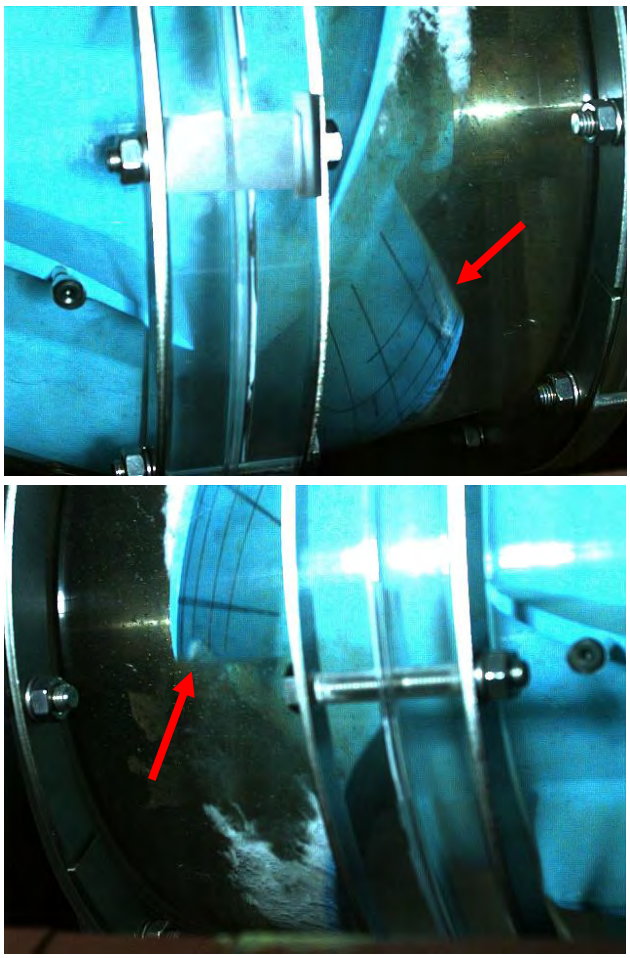

Figure 18 Pressure side leading edge sheet cavitation on both up-coming and down-going impeller blades.

By means of high speed video recordings, more details of the cavitation developments can be found. Figure 18 shows two pictures of high speed video recordings at 1850 frames per second for the 25.69 knots condition, where pressure side sheet cavitation has been observed in the lower half of each revolution. Although it is still difficult to judge if this cavitation will be erosive or not, generally it should be prevented. Seeing the present situation that no sheet cavitation has been observed on the suction side of the impeller blades, removing this pressure side sheet cavitation should not be a very difficult task by means of a new impeller blade design.

The present project with a selected pump from a standard series is a typical case where problems can be identified and prevented in the early design stage by model testing.

5 CONCLUSIONS AND RECOMMENDATIONS

Implementation of the ITTC recommended test procedures for waterjet systems has been discussed in detail by using a waterjet propelled 15 m Fast River Ferry as an example. Attention has been paid to scale effects of model testing and the method for Reynolds corrections.

From the tests, the pump head has been found to be less sensitive to Reynolds numbers, if the flow at the inlet of the pump is fully turbulent. However, impeller torque is highly Reynolds dependant. A rather high blade chord Reynolds number is generally needed before the test results can be reliably extrapolated to full scale. It is recommended to carry out the test at a blade tip chord Reynolds number as high as 4×10^6 to 5×10^6.

Strong Reynolds dependency of the apparent intake losses have also been found, which converges at a duct Reynolds number at 10^7. Detailed flow survey before the waterjet intake and at the pump inlet are essential for a correct prediction of the intake duct losses. Also important is a correct simulation of the boundary layer at the intake.

It is proposed to use the power loading coefficient to determine the operating point when the pump characteristics are extrapolated to full scale values. Cavitation inception can be carried out and expressed in the same way as for marine propellers with cavitation buckets, based on pump specific suction speed. High speed video observations on the pump cavitation can reveal detailed cavitation phenomena.

A final design waterjet system can reliably be tested, both for its efficiency as well as for its cavitation performance in the early design stage to prevent problems later.

5 ACKNOWLEDGEMENT

The authors are grateful for the valuable criticisms of Prof. Dr. Ir. T. van Terwisga to the draft of this paper.

REFERENCES

Arén P., Aartojärvi R. and Croner P. (1993). 'Review of test methods adopted for water jets at the KaMeWa Marine Laboratory'. Contribution to the 20th ITTC Workshop on Waterjets, San Francesco, U.S.A.

Brandner P.A. and Walker G.J. (2001). 'A waterjet test loop for the Tom Fink Cavitation Tunnel'. International Conference on Waterjet Propulsion III, RINA, Gothenburg, Sweden.

Chesnakas C.J., Donnelly M.J., Jessup S.D. and Lanni F. (2008). 'Testing waterjet at range of scales'. Proceedings of 27th Symposium on Naval Hydrodynamics, Seoul, Korea.

Chesnakas C.J., Donnelly M.J., Pfitsch D.W., Becnel A.J. and Schroeder S.D. (2010). 'Pump loop testing of an axial flow waterjet'. Proceedings of 28th Symposium on Naval Hydrodynamics, Pasadena, California.

Donnelly M. and Gowing S. (2008). 'Overview of recent development in testing of waterjets at NSWCCD'. Proceedings of Waterjet Propulsion 5, London, UK.

Fujisawa, N. (1995). 'Measurements of basic performances for waterjet propulsion systems'. International Journal of Rotating Machinery **2**(1), pp.43-50.

Hoshino T. and Baba E. (1993). 'Determination of propulsive performance of waterjet in model and full scale'. Contribution to the 20th ITTC Workshop on Waterjets, San Francesco, USA.

ITTC (2011). 'ITTC – Recommended procedure and guidelines – Propulsive performance prediction'. ITTC 7.5-02-05-03.1, revision 02, pp.1-9.

ITTC (2005). 'ITTC – Recommended procedure and guidelines – Testing and extrapolation methods, high speed marine vehicles – waterjets, waterjet system performance'. ITTC 7.5-02-05-03.2, revision 00, pp.1-10.

Kooiker K, van Terwisga T., Verbeek R. and van Terwisga P. (2003). 'Performance and cavitation analysis of a waterjet system on a cavitation tunnel'. Proceedings of International Conference on Fast Sea Transportation, Ischia, Italy.

Kruppa C.F.L. (1993). 'On pump installation Efficiency'. Contribution to the 20th ITTC Workshop on Waterjets, San Francesco, USA.

Kruppa C.F.L. (1996). 'Waterjet group – Final report and recommendations to the 21st ITTC'. Proceedings of the 21st ITTC Conference, Trondheim, Norway.

Lerbs H.W. (1951). 'On the effects of scale and roughness on free running propellers'. Journal of the American Society of Naval Engineers, Inc. **63**(1), February.

Liu R. (2010). 'Research on parametric design of duct system for marine waterjet propulsion'. Master Thesis of CSSRC, Wuxi. (in Chinese)

Purnell J. (2008). 'Waterjet inlet design and hull integration optimization for improved performance efficiency of an advanced waterjet'. CDI Marine Company, Report No. 841-3, Severna Park, MD, February.

Scherer O., Mutnick I. and Lanni F. (2001). 'Procedure for conducting a towing tank test of a waterjet propeller craft using LDV to determine the momentum and energy flux'. Proceedings of 26th ATTC, Webb Institute, July.

Tan D.Y., Miorini R.L., Keller J. and Katz J. (2012). 'Investigation of cavitation phenomena within an axial waterjet pump'. Proceedings of the Eighth International Symposium on Cavitation (CAV2012), Singapore.

Tan D.Y., Miorini R.L., Katz J. and Keller J. (2012). 'Cavitation phenomena within the rotor blade passage of an axial waterjet pump'. Proceedings of the 29th Symposium on Naval Hydrodynamics, Gothenburg, Sweden.

van Terwisga T. (2005). 'The special committee on validation of waterjet tests procedures – Final report and recommendations to the 24th ITTC'. Proceedings of the 24th ITTC Conference, Edinburgh, UK.